Inorganic Chemistry

Article

pubs.acs.org/IC

$Eu_9Cd_{4-x}CM_{2+x-y}\square_ySb_9$: $Ca_9Mn_4Bi_9$-Type Structure Stuffed with Coinage Metals (Cu, Ag, and Au) and the Challenges with Classical Valence Theory in Describing These Possible Zintl Phases

Nasrin Kazem,[†] Antonio Hurtado,[†] Benedikt Klobes,[‡] Raphaël P. Hermann,[‡,§] and Susan M. Kauzlarich*[,†]

[†]Department of Chemistry, University of California, One Shields Avenue, Davis, California 95616, United States

[‡]Peter-Grünberg Institute, JARA-FIT, Forschungszentrum Jülich GmbH, Jülich Centre for Neutron Science, D-52425 Jülich, Germany

[§]Faculté des Sciences, Université de Liège, B-4000 Liège, Belgium

Supporting Information

ABSTRACT: The synthesis, crystal structure, magnetic properties, and europium Mössbauer spectroscopy of the new members of the 9−4−9 Zintl family of $Eu_9Cd_{4-x}CM_{2+x-y}\square_ySb_9$ (CM = coinage metal: Au, Ag, and Cu) are reported. These compounds crystallize in the $Ca_9Mn_4Bi_9$ structure type (9−4−9) with the 4g interstitial site almost half-occupied by coinage metals; these are the first members in the 9−4−9 family where the interstitial positions are occupied by a monovalent metal. All previously known compounds with this structure type include divalent interstitials where these interstitials are typically the same as the transition metals in the anionic framework. Single-crystal magnetic susceptibility data indicate paramagnetic behavior for all three compounds with antiferromagnetic ordering below 10 K (at 100 Oe) that shifts to lower temperature (<7 K) by applying a 3 T magnetic field. ^{151}Eu Mössbauer spectra were collected on polycrystalline powder samples of $Eu_9Cd_{4-x}CM_{2+x-y}\square_ySb_9$ at 50 and 6.5 K in order to evaluate the valence of Eu cations. Although the Zintl formalism states that the five crystallographically distinct Eu sites in $Eu_9Cd_{4-x}CM_{2+x-y}\square_ySb_9$ should bear Eu^{2+}, the Mössbauer spectral isomer shifts are clearly indicative of both 2+ and 3+ valence of the Eu cations with the Cu- and Au-containing compounds showing higher amounts of Eu^{3+}. This electronic configuration leads to an excess of negative charge in these compounds that contradicts the expected valence-precise requirement of Zintl phases. The spectra obtained at 6.5 K reveal magnetic ordering for both Eu^{2+} and Eu^{3+}. The field dependence of Eu^{2+} indicates two distinct magnetic sublattices, with higher and lower fields, and of a small field for Eu^{3+}. The site symmetry of the five Eu sites is not distinguishable from the Mössbauer data.

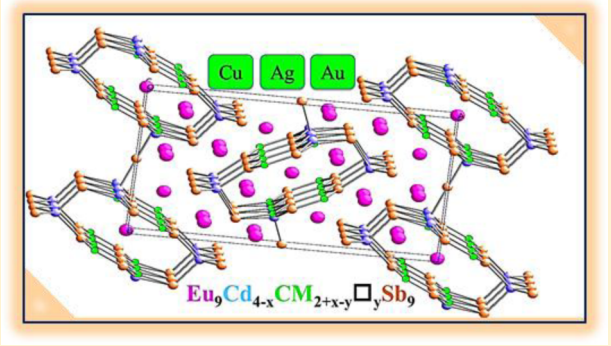

1. INTRODUCTION

Zintl phases are traditionally defined as compounds made of main-group electropositive metals and electronegative main-group elements. It is conventionally assumed that the electrons are donated from the electropositive metals to the more electronegative elements similar to the salt-like structures but not sufficient to satisfy the octet rule by the more electronegative elements.[1,2] As a result, the electronegative elements complete a filled valence electron configuration through covalent bonding by making anionic networks. This description considers the electropositive elements as charge-balancing "spectators" that fill the voids made in the anionic network. In contrast to the traditional description of Zintl phases, various nonclassical Zintl compounds, called polar intermetallic phases, can be formed via integration of transition and rare-earth metals replacing the more electropositive main-group or alkali or alkaline-earth elements, respectively. These transition- or rare-earth-metal-containing phases can be described as Zintl structures, showing that Zintl phases are not limited to elemental compositions with large electronegativity difference. As a result, a wide variety of materials with bonding/electronic structure between that of insulators and metals are possible.[1] Although these results show that the bonding/electronic structure understanding of Zintl phases is oversimplified, new nonclassical structures can be still rationalized by using the simple electron counting rules provided by the Zintl concept. In recent years, Zintl phases have attracted great attention because the flexibility and complexity of their structures make their electronic properties suitable for tuning within a structure type by either isovalent or aliovalent elemental substitutions. The high flexibility of the structures makes Zintl phases a

Special Issue: To Honor the Memory of Prof. John D. Corbett

Received: August 24, 2014
Published: October 29, 2014

Table 1. Selected Crystal Data and Structure Refinement Parameters for $Eu_9Cd_{4-x}CM_{2+x-y}\square_ySb_9$

empirical formula	$Eu_9Cd_{3.70}Cu_{0.30(1)}Cu_{1.17(1)}Sb_9$	$Eu_9Cd_{3.95}Ag_{0.05(1)}Ag_{1.12(1)}Sb_9$	$Eu_9Cd_{3.78}Au_{0.21(4)}Au_{1.02(1)}Sb_9$
fw (g/mol)	2972.92	3033.69	3132.64
data collection temp (K)	90(2)	90(2)	90(2)
radiation	Mo Kα	Mo Kα	Mo Kα
cryst size (mm^3)	0.06 × 0.06 × 0.02	0.04 × 0.05 × 0.03	0.12 × 0.11 × 0.02
cryst syst	orthorhombic	orthorhombic	orthorhombic
space group	*Pbam* (No. 55)	*Pbam* (No. 55)	*Pbam* (No. 55)
unit cell dimens			
a (Å)	22.8479(10)	23.0077(15)	22.9391(33)
b (Å)	12.9197(6)	12.9074(9)	12.9429(19)
c (Å)	4.7199(2)	4.7600(3)	4.7455(7)
unit cell volume ($Å^3$), *Z*	1393.26, 2	1413.58, 2	1408.93, 2
density (F_{calc}, g/cm^3)	7.086	7.127	7.384
abs coeff μ (mm^{-1})	32.29	31.72	37.32
final *R* indices [$F_o > 4\sigma(F_o)$]	R1 = 0.0176 (2499 data), wR2 = 0.0320 (2499 data)	R1 = 0.0139 (1884 data), wR2 = 0.0257 (1884 data)	R1 = 0.0195 (2794 data), wR2 = 0.0399 (2794 data)
final *R* indices [all data]	R1 = 0.0206 (2702 data), wR2 = 0.0329 (2702 data)	R1 = 0.0157 (1987 data), wR2 = 0.0265 (1987 data)	R1 = 0.0199 (2828 data), wR2 = 0.0401 (2828 data)
largest peak/hole ($e^-/Å^3$)	1.40/−1.16	1.14/−1.06	3.37/−2.75

treasured area for thermoelectric studies with phases such as $Eu_{11}Cd_6Sb_{12-x}As_x$,[3] $Yb_{14}Mn_{1-x}Al_xSb_{11}$,[4] $Yb_{13.6}La_{0.4}MnSb_{11}$,[5] and $Yb_{1-x}Ca_xZn_2Sb_2$,[6] where the transport properties can be precisely altered by means of substitutional alloying.[7,8] This flexibility in structure provides a wide range of materials such as Mn^{2+}- and Al^{3+}-containing $Yb_{14}Mn_{1-x}Al_xSb_{11}$ compounds or $Yb_{13.6}La_{0.4}MnSb_{11}$ in which La^{3+} occupies Yb^{2+} sites while the anionic networks remain intact. This raises the question of how well the Zintl approach can explain the bonding within intermetallic phases. In many cases, the presence of mixed-valence elements or the presence of interstitials make the Zintl formalism seem less effective for intermetallic phases. Here, we will focus on a class of $Eu_9Cd_{4-x}CM_{2+x-y}\square_ySb_9$ (CM = coinage metals: Cu, Ag, and Au) compounds whose stability is attributed to the presence of interstitial ions.

The isostructural family of $AE_9TM_4Pn_9$ (AE = Ca and Sr; TM = Zn, Cd, and Mn; Pn = Sb and Bi), the so-called 9−4−9 phases, was first reported by Brechtel et al. in 1979 and 1982, introducing $Ca_9Mn_4Bi_9$ as a new structure type.[9] On the basis of the single-crystal X-ray diffraction studies, all of the $AE_9TM_4Pn_9$ compounds were presented as fully stoichiometric compositions with no suggestions of off-stoichiometry regardless of very high *R* values. In 2001, Kim et al. showed that by using certain lanthanide ions that bear mixed valency some novel and exotic anionic networks can be stabilized, which can result in unusual electronic phenomena.[10] $Yb_9Zn_4Bi_9$ crystallizes in the $Ca_9Mn_4Bi_9$ structure type, and magnetic property measurements revealed the presence of one Yb^{3+} per formula unit, with the remainder being Yb^{2+}, in good agreement with the density functional theory (DFT) band calculation, a result consistent with the Zintl formalism for a valence-precise compound. This raised the question concerning the structure and bonding for the previously reported $Ca_9Zn_4Bi_9$ with the possibility of nonstoichiometry as likely so that the charge balance would be satisfied. In 2004, this prediction was confirmed by Bobev et al. by reexamining the structures of the 9−4−9 family with the study of the $Ca_9Zn_4Sb_9$ compound as the archetype.[11] These studies resulted in a nonstoichiometric formula of $Ca_9Zn_{4.5}Sb_9$, making it a valence-precise compound, as predicted by Kim et al. In this study, a Yb analogue of $Ca_9Zn_{4.5}Sb_9$ was successfully synthesized, but attempts to make $Yb_9Zn_4Sb_9$ remained unsuccessful. Although charge balance could be achieved by mixed valency of Yb, it was shown that the charge balance was maintained by the interstitial substitution of Zn to make a nonstoichiometric composition of $Yb_9Zn_{4.5}Sb_9$. The small magnetic moment observed for $Yb_9Zn_{4.5}Sb_9$, ∼0.16 μ_B/Yb (Yb^{3+} has a magnetic moment of ∼4.5, and Yb^{2+} has no magnetic moment), was attributed to a possible Yb^{3+} impurity, and it was concluded that all of the Yb ions in $Yb_9Zn_{4.5}Sb_9$ are Yb^{2+}. Such compounds with one-electron donation from interstitial sites are expected to be narrow-gap semiconductors based on DFT calculations. As additional studies, Bobev in 2007 and 2010 made a family of $A_9TM_{4+x}Pn_9$ (A = Ca, Sr, Eu, and Yb; TM = Mn, Cd, and Zn; Pn = Sb and Bi) compounds where the interstitial positions were occupied by divalent TM^{2+} ions with the same transition-metal type in the framework.[12,13] This work showed that there is a narrow homogeneity range for all of these compounds that is a result of the interplay between the size and electronic effects.[12] We report here the discovery of the first coinage-metal-containing 9−4−9 phases $Eu_9Cd_{4-x}CM_{2+x-y}\square_ySb_9$, in which the interstitial cavities are filled by monovalent ions and there is additional mixed occupancy of one of the Cd sites. These new compounds can be considered stuffed 9−4−9 structures. We will discuss the synthesis, structural characterization, and magnetic properties of these compounds along with the valence of the rare-earth metal (Eu) in order to better understand the nature of the bonding in this family.

2. EXPERIMENTAL SECTION

Synthesis. $Eu_9Cd_{4-x}CM_{2+x-y}\square_ySb_9$ compounds were initially synthesized accidently as reaction products of Eu, Cd, CM, and Sb in Sn flux[14] (ratio of Eu:Cd:CM:Sb:Sn = 11:6−x_{syn}:x_{syn}:12:30; x_{syn} = 2) in an effort to synthesize solid solutions of $Eu_{11}Cd_{6-x}CM_xSb_{12}$ and thus to tune the thermoelectric properties of $Eu_{11}Cd_6Sb_{12}$[15] as reported previously.[3] The combination of elements was heated at 100 °C/h to 500 °C and allowed to dwell for 6 h before heating at 100 °C/h to 950 °C and dwelling for 96 h. Subsequently, the reaction vessels were slowly cooled at 5 °C/h to 600 °C, at which point molten Sn was removed by inverting and placing the reaction vessels in a centrifuge and rotating for 2−3 min at 6500 rpm. Last, the reaction containers were opened in a N_2-filled glovebox equipped with an optical microscope and at moisture levels below 1 ppm. Silver, reflective

dx.doi.org/10.1021/ic502061w | Inorg. Chem. 2015, 54, 850−859

crystals were later identified as $Eu_9Cd_{4-x}CM_{2+x-y}\square_ySb_9$ belonging to the $Ca_9Mn_4Bi_9$ type (Pearson's symbol oP44) in which traditionally so-called interstitial 4g sites are partially occupied by a coinage metal (Cu, Ag, and Au). After identification of the $Eu_9Cd_{4-x}CM_{2+x-y}\square_ySb_9$ structure by X-ray crystallography, the reactions were repeated with the ratio of Eu:Cd:CM:Sb:Sn = 9:3.5:1.5:9:23, scaled for 5 g of Sn.

Single-Crystal X-ray Diffraction. Multiple crystals of a variety of shapes from each reaction were studied by single-crystal X-ray diffraction to characterize the products. The crystals were selected under a microscope in Paratone N oil. Then, if necessary, the crystal was cut to the desired dimensions for data collection. Selected crystals were positioned on the tops of glass fibers or MiTeGen microloops, quickly transferred to the nitrogen stream, and mounted on the goniometer. Diffraction data for all of the crystals were collected at 90 K on a Bruker Apex II diffractometer with graphite-monochromated Mo Kα radiation (λ = 0.71073 Å) and a CCD area detector. Several sets of ω scans (0.3°/frame) at different Φ settings were collected while in a nitrogen stream. Determinations of the unit cell parameters, refinements, and raw frame data integration were completed using the *APEX II*, version 2011.4-1, software. The space group was determined on the basis of systematic absences using *XPREP*, and the structure was solved using direct methods from the *SHELXTL*, version 6.14, package. After successful assignments of the high electron density peaks as Eu, Cd, and Sb, the value of R reached ~9% with a large residual peak near Sb2 in all compounds. By assignment of this peak as the CM atom, the large atomic displacement parameter values for all of the CM sites suggested partial occupancy of these elements at the interstitial sites, further improving the R value to ~5%. In Cu-substituted compounds, Cd1 showed high atomic displacement parameter values, interpreted as evidence of mixed occupancy with a lighter atom. The R value improved to ~4.5% by considering Cd1 as mixed occupancy of Cd and Cu while requiring the refinement of the occupancy site to be 1 with the same isotropic atomic displacement parameter values for the mixed elements. However, a residual peak close to the Cd1 site, which could not be completely removed by anisotropic atomic displacement parameter refinements, was better interpreted as a different center of mass for the mixed elements. Providing the unrestricted positional refinement for the two elements improved the R value from 4.5% to ~3.0%, which was reduced further to 1.7% with anisotropic refinement, resulting in no significant residual peaks in the difference Fourier maps (Table 1). Applying an unrestricted atomic displacement parameter refinement for the two sites made the refinement unstable, so the atomic displacement parameter values were restricted to be the same for the mixed elements. The same refinement procedures were followed for the other compounds. Although it was not possible to distinguish Ag from Cd by the X-ray diffraction technique, the lower occupied site was assigned as Ag, in order to be consistent with the structural solution for the Cu- and Au-containing compounds. Occupancies of the shared CM/Cd1 sites were fixed to fully fill the crystallographic site, and they were assigned the same atomic displacement parameters. The CIFs are provided in the Supporting Information (SI).

Magnetic Properties. The temperature dependence of the magnetic susceptibility for $Eu_9Cd_{4-x}CM_{2+x-y}\square_ySb_9$ was collected in a Quantum Design MPMS2 SQUID from 2 to 300 K in a magnetic field (μ_0H) of 3 T. Single crystals of $Eu_9Cd_{4-x}CM_{2+x-y}\square_ySb_9$ were selected and secured using Kapton tape in a common drinking straw in the glovebox. The collected data were converted to molar magnetic susceptibility [$\chi(T) = M/H$] in emu/mol units.

Electron Microprobe Analysis (EMPA). Single crystals used for magnetic property measurements were enclosed in epoxy and polished to provide flat surfaces for analysis. The polished samples were mounted on 25 mm metal rounds using adhesive carbon tape and were carbon-coated to make them conducting. Microprobe analysis was performed using a Cameca SX-100 electron probe microanalyzer with wavelength-dispersive spectrometers. Characteristic X-rays emitted by the samples were analyzed by wavelength-dispersive spectroscopy to determine the compositions of the samples, and element mapping was accomplished to assess the spatial distribution of the elements in the samples. The X-ray intensities of Eu, Cd, Cu, Ag, Au, Sb, and Sn were compared with the calibrated standards $EuPO_3$, Cd (metal), Cu (metal), Ag (metal), Au (metal), Sb (metal), and Sn (metal) for quantitative analysis. At least 15 different points with a spot size of 1 μm were analyzed for each sample.

Mössbauer Spectroscopy. The ^{151}Eu Mössbauer spectra were obtained on a constant-acceleration spectrometer using a 25 mCi $^{151m}SmF_3$ source. The velocity calibration was performed with α-Fe at room temperature utilizing a ^{57}Co/Rh source. All Mössbauer spectra presented herein were obtained using powdered samples placed in a Janis SH-850 cryostat, and the extracted isomer shifts are reported with reference to EuF_3 at 300 K.

3. RESULTS AND DISCUSSION

Structures and Compositions. These compounds can be envisioned as being crystallized in the $Ca_9Mn_4Bi_9$ structure type,[9] where the interstitial position (4g Wyckoff site) is partially occupied by coinage metals. All of the structures correspond to the orthorhombic space group *Pbam* (No. 55) with unit cell parameter ranges of a = 22.8479−23.077 Å, b = 12.9074−12.9429 Å, and c = 4.7199−4.7600 Å and Z = 2. The details of data collection and crystal structure refinements are given in Table 1. In order to build up the structure within this structure type, we first describe the framework and then how the interstitials are placed therein. The structure can be initially imagined as a hypothetical composition of $Eu_9Cd_4Sb_9$, with the structure of $Ca_9Mn_4Bi_9$ where the interstitial positions are unoccupied and indicated by green circles, as shown in Figure 1. In this image, the four corner-shared tetrahedral units of

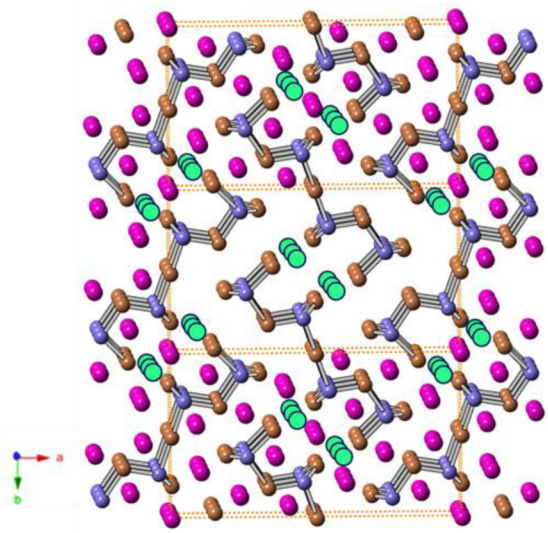

Figure 1. View of the crystal structure of the hypothetical $Eu_9Cd_4Sb_9$ with the structure of $Ca_9Mn_4Bi_9$ down the c axis. The interstitial sites in this structure are shown as green spheres. Eu, Cd, and Sb ions are shown in pink, blue, and orange, respectively. Eu ions are removed from the central unit cell for clarity.

$CdSb_4$ are connected to each other in the *ab* plane to make one-dimensional $[Cd_4Sb_9]^{19-}$ ribbonlike chains that are running parallel to the c direction. These chains make a two-dimensional structural feature by connecting the first and last two units of $CdSb_4$ of the two adjacent ribbons through filling of the interstitial sites. In this way, a channel is made in the *ab* plane and running in the c direction that is occupied by Eu^{2+} cations. These channels are connected to each other to make a chain of channels running in the b direction by rather rare long linear Sb−Cd−Sb bonds. A unit cell of the structure of the

dx.doi.org/10.1021/ic502061w | *Inorg. Chem.* 2015, 54, 850−859

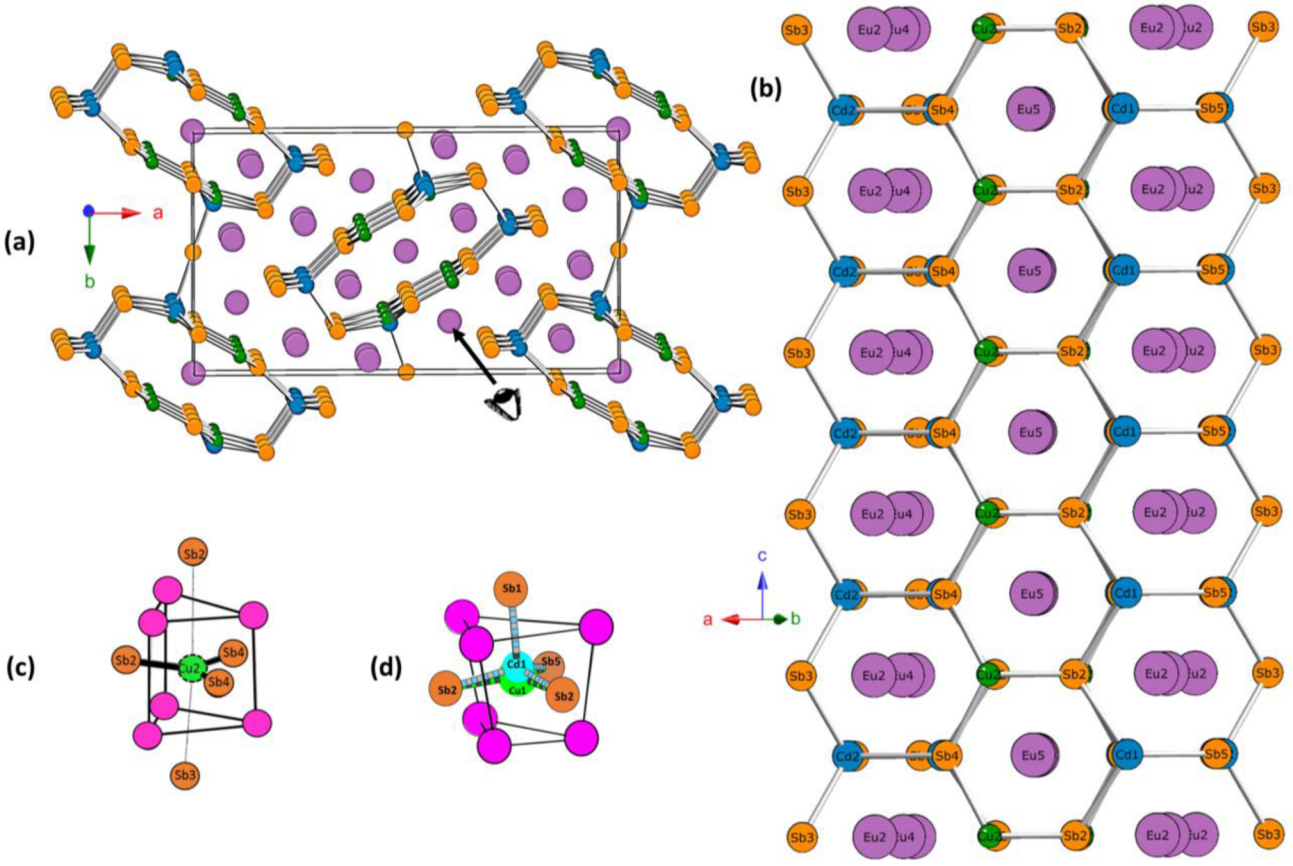

Figure 2. (a) View of one unit cell of the hypothetical $Eu_9Cd_{4-x}Cu_{2+x}Sb_9$ in the *c* direction. (b) One-dimensional ribbonlike chain running in the *c* direction made of the connected hexagonal planar units in the hypothetical $Eu_9Cd_4Cu_2Sb_9$ in which only the interstitial position (Cu2) is occupied by coinage metals (Cu here) seen in the [*u*, *v*, *w*] = [1, 3, 0] direction shown by the arrow and eye icon in part a. (c) View of the coordination environment of the interstitial site (Cu2 site). The coinage metal holds distorted trigonal-planar geometry at this site. (d) View of the coordination environment of the TM1 site; unlike Cd1, the coinage metal (Cu1) tends to stay in the trigonal plane made by Sb2−Sb5−Sb2 rather than in tetrahedral geometry. The Cu, Cd, Sb, and Eu ions are shown in bright green, blue, orange, and pink, respectively.

Table 2. Fractional Coinage Metal Occupation at the Interstitial Position and Cd Sites and also Comparisons of Elemental Analysis from Single-Crystal X-ray Diffraction and EMPA from Single Crystals of $Eu_9Cd_{4-x}CM_{2+x-y}\square_ySb_9$

single-crystal X-ray diffraction				EMPA (single crystal)
composition	SOF at CM3 (%)	tendency for mixed occupancies at the Cd sites	electron excess/defect based on the simple valence electron count	composition
$Eu_9Cd_{3.70}Cu_{1.46(1)}Sb_9$	58.4 (±3)	15.0 (±6)% in Cd1	3(9.00) − [2(9.00) + 2(3.70) + 1.46] = 0.14(1)	$Eu_{9.04(3)}Cd_{3.75(3)}Cu_{1.45(3)}Sb_{9.05(2)}$
$Eu_9Cd_{3.95}Ag_{1.15(1)}Sb_9$	56.0 (±2)	1.3 (±6)% in Cd1	3(9.00) − [2(9.00) + 2(3.95) + 1.146] = −0.05(1)	$Eu_{9.03(5)}Cd_{3.80(5)}Ag_{1.42(4)}Sb_{9.05(4)}$
$Eu_9Cd_{3.79}Au_{1.23(1)}Sb_9$	51.0 (±1)	10.6 (±3)% in Cd1	3(9.00) − [2(9.00) + 2(3.79) + 1.23] = 0.19(1)	$Eu_{9.07(6)}Cd_{3.86(3)}Au_{1.28(3)}Sb_{9.08(3)}$

hypothetical $Eu_9Cd_{4-x}Cu_{2+x}Sb_9$ as the archetype of the $Eu_9Cd_{4-x}CM_{2+x}Sb_9$ compounds where the interstitial position is fully substituted by a coinage metal is shown in Figure 2a. In the case of full occupation by Cu^{1+} ions at the interstitial sites, the formed two-dimensional features are $[Cd_4Cu_2Sb_9]^{17-}$ with one electron lower than the 18 electrons donated by Eu^{2+} ions, suggesting that the optimum composition should be reached by the half-occupancy of Cu^+ interstitials if electronic effects govern the formation of these systems. When the hypothetical $Eu_9Cd_{4-x}Cu_{2+x}Sb_9$ structure is viewed in Figure 2b in the [*u*, *v*, *w*] = [1, 3, 0] direction, shown by the arrow and eye icon in Figure 2a, it becomes apparent that the $Eu_9Cd_{4-x}Cu_{2+x}Sb_9$ compound adopts a fragment made of hexagonal moieties formed by Cu−Cd−Sb atoms, running in the *c* direction, which will be discussed later. These hexagonal moieties are making the body of each tunnel running in the *c* direction discussed earlier. Note that the Cu1 atoms are removed in Figure 2b, and only Cd atoms are shown in the Cd1 position for more clarity, leading to a composition of $Eu_9Cd_4Cu_2Sb_9$.

The $Ca_9Mn_4Bi_9$ structure contains five cation sites (Ca here), five Pn sites (Bi here), and two transition-metal sites (Mn here). The interstitially stabilized family of $A_9TM_{4+x}Pn_9$ contains an additional transition-metal site, TM3, called the interstitial site. In the $Eu_9Cd_{4-x}CM_{2+x-y}\square_ySb_9$ compounds, the interstitial position is exclusively occupied by coinage metals. So, the difference between the 9−4−9 structure of $Ca_9Mn_4Bi_9$ and the interstitially stabilized structures is the fractional occupation in this new third transition-metal site (TM3). The coordination of this interstitial position is shown in Figure 2c. The coordination geometry of this interstitial site (TM3) is not tetrahedral, as in the Cd sites (TM1 and TM2), but a rare trigonal-planar coordination, as seen in the EuCMSb phases[16]

dx.doi.org/10.1021/ic502061w | *Inorg. Chem.* 2015, 54, 850−859

as well. This interstitial position is placed at the center of a trigonal prism made by six Eu ions that are connected to three Sb ions capping the five faces of the trigonal prism. The refined site occupancies for the interstitial position obtained from single-crystal X-ray diffraction data, listed in Table 2, show that a similar fraction of this crystallographic site is substituted by coinage metals for all compounds regardless of their different covalent radii, Cu (1.22 Å), Ag (1.36 Å), and Au (1.30 Å).[17] In structural studies of transition-metal-containing phases ($A_9TM_{4+x}Pn_9$),[11,13] the occupational fraction at the interstitial position depends on the size of the interstitial hole, and for a given interstitial vacancy size, it mainly depends on the size of the interstitial ion.[12] For example, the Cd interstitial occupancy fraction in $Eu_9Cd_{4+x}Bi_9$ is almost half of that of Zn in $Yb_9Zn_{4+x}Sb_9$, while their void size is almost the same (the ratio of the cation to pnicogen radii controls the size of the cavity).[12] It is the approximately 15% size difference of Cd and Zn that leads to this variance.[17] Although Cu and Ag have very similar size difference (~12%) compared to Zn and Cd mentioned above, the fractional interstitial occupancy by Ag ions (~56%) is similar to the fractional interstitial occupancy by Cu (~58%) in $Eu_9Cd_{4-x}CM_{2+x-y}\square_ySb_9$, as shown in Table 2. This suggests that factors other than the size have a primary role controlling electronics and structure in these coinage metal compounds, unlike the transition-metal-containing interstitial compounds in this family that are known so far.

As shown in Table 2, all of the refined site of occupancies showed that coinage metals occupy the interstitial position at a level of more than 50%, the theoretical maximum occupancy of a monovalent interstitial atom required to make a valence-precise compound. For all samples, there is always additional electron density (ca. 8−10 $e^-/Å^3$) located approximately 0.65 Å away from Cd1. This extra electron density was modeled as a disorder introduced by the fractional occupancy of coinage metals, which is noncoincident with the Cd1 site in a way that the sum of the occupancy at Cd1 and the coinage metal site adds up to full occupancy. This model improved the *R* value from approximately 5% to 3% and provided a featureless final difference Fourier map. Among the compounds, Cu has the highest tendency to occupy the Cd1 position (~15%) and Ag has the lowest. However, this perceived affinity of a particular CM for occupying the Cd1 site (~1%) might simply be a result of the inability of the X-ray technique to distinguish between Ag and Cd because they have only a one-electron difference. In Figure 2d, it is clear that the coinage metal at the Cd1 site deviates from being in tetrahedral coordination by Sb ions and prefers trigonal-planar geometry. This pseudomixed occupancy at the Cd1 site may be the reason for occupation in the interstitial position being more than necessary to satisfy the valence balance. Therefore, higher occupation at the interstitial site provides more electrons to balance the charges in this compound. The highest occupational factor at the interstitial position for the Cu-containing analogue may be due to the higher affinity of Cu^+ to occupy some Cd^{2+} sites at the Cd1 site compared to Ag and Au. There is no evidence of coinage metal mixed occupancy at the Cd2 site. This might be because of the shorter Cd−Sb bond lengths at the Cd2 sites (2.81, 2.83, and 2.82 Å for Cu, Ag, and Au, respectively) compared to the longer Cd−Sb bond lengths at the Cd2 site (3.05, 3.04, and 3.03 Å for Cu, Ag, and Au, respectively), especially the long Cd1−Sb3 bond, which likely facilitates substitution of the larger atom. The final compositions for each sample are given in Table 1; the fractions of the coinage metals at the Cd1 and interstitial sites are shown separately (the fraction of coinage metals coming from substitution at the Cd1 site is shown in bold). As shown in Table 2, the electron count cannot be explained based on the compositions from both single-crystal X-ray diffraction and EMPA; e.g., the composition from single-crystal X-ray diffraction of the Cu analogue $(Eu^{2+})_{9.00}(Cd^{2+})_{3.70}(Cu^{1+})_{1.46}(Sb^{3-})_{9.00}$ leads to 26.86 electrons donated by metal cations, which is close to the 27 electrons needed by the Sb ions in the anionic framework but still slightly deficient. The Ag analogue shows the least deviation from the Zintl concept (slightly electron-rich). The amount of Ag might be underestimated as the limitation of the X-ray technique to evaluate the Ag concentration at the Cd sites. However, all of the compositions from EMPA show off-stoichiometry by the lack of electrons for the valence-precise compound. In this way, it can be assumed that all of the compounds are close to being valence-precise and that the interstitial sites are populated by the coinage metals (regardless of their size) to provide enough electrons to ensure charge balance.

Another aspect of crystallography that deserves special attention relates to the extent of deviation from trigonal-planar geometry for coinage metals at both the interstitial and Cd1 sites. The positions of the coinage metals at the interstitial sites and Cd1 site (it is not exactly coincident with the Cd1 site) are shown in Figure 2a. In this structure, it is assumed that the interstitial site is fully occupied by coinage metal, Cu here. The coinage metal, Cd1, and Cd2 sites then constitute the three corners of the hexagon made by Cd/Cu−Sb bonds. To make a perfect hexagon, the angles between Sb−Cd and Cu−Sb should be 120°. The refined positions of coinage metals at the vicinity of the Cd1 and interstitial sites reveal that the Ag-containing compound is the one with the least deviation from 120°, whereas Cu is the one with the highest deviation. All of the angles for the Sb−Cd−Sb features are listed in Table 2. A careful look at these positions reveals that, even though Ag seems to keep the ideal 120° angle at both the interstitial position and Cd1 site, it actually deviates the most from the plane made by the three Sb ions at the interstitial position. The coinage metal distances from the Sb trigonal planes and bond lengths are given in Table 3. Although at the Cd1 site the bond lengths are very similar, in the interstitial position, the CM−Sb2 interaction is very short, whereas the other two CM−Sb4 interactions are longer. These geometries might affect the properties of these compounds because the trigonal-planar geometry can accommodate a hexagonal geometry, reminding one of graphene-style fragments. These sheets suggest charge-transport anisotropy in the *c* direction (see Figure 2b) and may

Table 3. Angles of Sb−CM−Sb Species from the Single-Crystal X-ray Diffraction in $Eu_9Cd_{4-x}CM_{2+x-y}\square_ySb_9$

	Cu	Ag	Au
2(Sb2−CM1−Sb2) (deg)	114.8	118.8	116.0
Sb5−CM1−Sb2 (deg)	120.6	120.6	120.6
Sb2−CM2−Sb4 (deg)	117.3	119.0	118.6
2(Sb4−CM2−Sb4) (deg)	124.9	121.0	122.5
Sb2−CM2 (Å)	2.515	2.601	2.568
2(Sb4−CM2) (Å)	2.662	2.773	2.706
Sb5−CM1 (Å)	2.742	2.777	2.798
2(Sb2−CM1) (Å)	2.801	2.774	2.759
CM1 (deviation from the trigonal plane)	0.32	0.13	0.27
CM2 (deviation from the trigonal plane)	0.09	0.15	0.08

dx.doi.org/10.1021/ic502061w | Inorg. Chem. 2015, 54, 850−859

provide a pathway for electron transport in the [0, 0, 1] direction. A comparison of the properties of the stuffed and unstuffed compounds would be required to assess this suggestion.

Magnetic Properties. The rare geometry of coinage metals at both the interstitial position and the Cd1 site invites inquiry into their oxidation states. In order to provide a better understanding of the structure and the electronic properties of these compounds, magnetic property measurements were carried out on the single crystals. The X-ray maps of the single crystals used for magnetic studies, shown in Figure S1 in the SI, demonstrate that these are all high-quality crystals belonging to the 9−4−9 family, and their compositions are well-matched with the compositions from single-crystal X-ray diffraction. A higher content of Ag was detected, compared with that determined from the single-crystal X-ray structure, consistent with ∼0.2 Ag ions/formula (10% site of occupancy) at the Cd1 site. Figure 3 shows zero-field-cooled (ZFC) and field-cooled

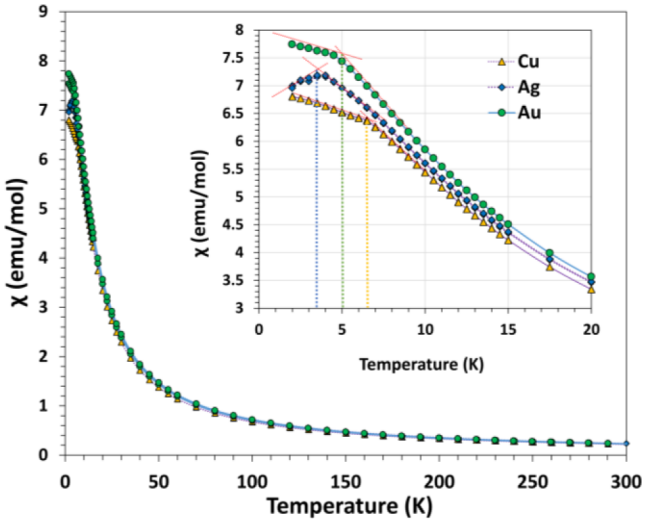

Figure 3. Temperature dependence of the magnetic susceptibility $\chi(T) = M/H$ for $Eu_9Cd_{4-x}CM_{2+x-y}\square_ySb_9$ measured under applied field of 3 T. The upper inset shows a closer look at the magnetic transition temperature so that the cusps are more apparent.

(FC) magnetic susceptibility (χ) as a function of the temperature (T) for the three coinage-metal-stuffed 9−4−9 compounds carried out from 2 to 300 K and at 3 T. The magnetic behavior of all of the compounds is similar. The inverse susceptibility ($1/\chi$) as a function of the temperature (T) for the three coinage-metal-stuffed 9−4−9 compounds are shown in Figure S2 in the SI. All samples exhibit an antiferromagnetic-like transition, consistent with the previously reported $Eu_9Cd_{4.2}Bi_9$,[12] where this transition temperature decreases with increasing size of the unit cell, so that Cu and Ag have the highest and lowest T_N (Néel temperature) values of 6.5 and 3.5 K, respectively; the inset in Figure 3 shows the data in the low-temperature regime. The inverse susceptibility, $\chi^{-1}(T)$, follows the Curie−Weiss law $\chi(T) = C/(T - \theta_P)$, where C is the Curie constant and θ_P is the Weiss temperature, as reported in Table 4. The calculated θ_P values are similar in magnitude to the antiferromagnetic transition temperatures, and their negative signs support the assignment of the downturn in the magnetic susceptibility data as antiferromagnetic in nature. This is additionally supported by the fact that the ZFC/FC magnetic susceptibility data are superimposable. The effective magnetic moments (μ_{eff}) for each of the compounds are obtained by the calculated Curie constants $\mu_{eff} = 2.48C^{1/2}$ from the fit in the temperature range 50−300 K (the paramagnetic regime) and listed in Table 4 along with the estimated number of Eu^{2+}/formula through the $N_{Eu^{2+}} = (\mu_{eff}/7.94)^2$ equation. For the Ag compound, $\mu_{eff} \approx 7.9(1)/Eu$ is in excellent agreement with the theoretical magnetic moment for free Eu^{2+} ions according to $\mu_{eff} = g[j(j + 2)] = 7.94\ \mu_B$, suggestive of 8.9(3) Eu^{2+}/formula. These results suggest the presence of a nonmagnetic oxidation state of 1+ for Ag because monovalent coinage metals provide an electronic structure of fully filled orbital shells (d^{10} ions) with no contribution to the paramagnetic moment. This result is consistent with the common oxidation state of 1+ for Ag because Ag^{II} and Ag^{III} are rare. Cu- and Au-containing analogues exhibit lower μ_{eff} values than the Ag analogue. In $Eu_{9.04}Cd_{3.75}Cu_{1.46}Sb_{9.05}$, the ions possibly contributing to the magnetic moment are Eu^{2+}, Cu^{2+}, and Au^{2+} with μ_{eff} = 7.94, ∼2.0, and ∼3.7 μ_B, respectively. The lower measured magnetic moment suggests the presence of Eu^{3+} with the ground state of zero magnetic moment. The experimental μ_{eff}/Eu of 7.65(5) and 7.75(1) for the Cu- and Au-containing analogues, respectively, suggests the presence of ∼0.7(1) and 0.4(3) Eu^{3+}/formula unit (i.e., ∼3.0 and 1.7 atomic %) if all of the Cu and Au are nonparamagnetic CM^+; otherwise, a higher content of Eu^{3+} is expected. These results for Cu- and Au-containing compounds are contrary to what a simple valence electron count suggests for a Zintl phase. The electronic structure studies on the other members in the 9−4−9 family indicated that the polyanionic network requires 19 electrons, while only 18 electrons are donated by the cations.[12] So, the occupation at the interstitial sites is as a result of this one-electron deficiency. The presence of ∼1 Eu^{3+} can itself complete this electron deficiency to donate the necessary 19 electrons to the polyanionic network to optimize the bonding. One might expect that there should not be interstitial ions because the required valence-precise condition for a Zintl phase is already achieved, similar to $Yb_9Zn_4Sb_9$, where ∼0.9 Yb^{3+}/formula makes a valence-precise compound.[10] Mössbauer spectroscopy is able to evaluate the local electronic structure around Mössbauer-active isotopes via hyperfine interactions with the nearby electrons that act on the nuclear levels. As a result, Eu Mössbauer spectroscopy was carried out to elucidate the local atomic/electronic structure around the resonant Mössbauer Eu ions and in order to assess its valence and explain this ambiguity.

Table 4. Magnetic Data for $Eu_9Cd_{4-x}CM_{2+x-y}\square_ySb_9$ (CM = Au, Ag, and Cu)

		T_N (K)				
compound	θ (K)	0.1 T	3 T	μ_{eff}/formula (measd) (μ_B/f.u.)	μ_{eff}/Eu^{2+}	no. of Eu^{2+}/formula
$Eu_{9.04(3)}Cd_{3.75(3)}Cu_{1.46(3)}Sb_{9.05(2)}$	−3.0(2)	9.5	6.5	22.9(1)	7.64(5)	8.3 (±1)
$Eu_{9.03(5)}Cd_{3.80(5)}Ag_{1.42(4)}Sb_{9.05(4)}$	−2.4(1)	8.5	3.5	23.7(4)	7.9(1)	8.9 (±3)
$Eu_{9.07(6)}Cd_{3.86(3)}Au_{1.28(3)}Sb_{9.08(3)}$	−4.5(4)	9	5	23.2(4)	7.7(1)	8.6 (±3)

dx.doi.org/10.1021/ic502061w | Inorg. Chem. 2015, 54, 850−859

^{151}Eu Mössbauer Spectral Results. ^{151}Eu Mössbauer spectra obtained at 50 and 6.5 K are shown in Figure 4a,b; the

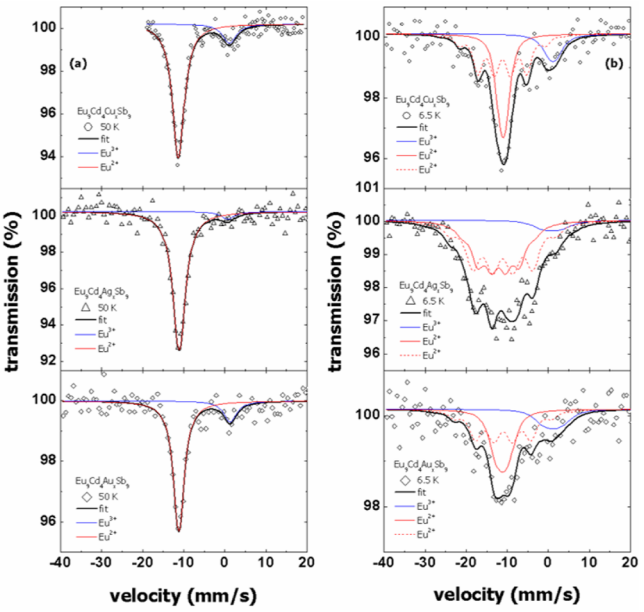

Figure 4. (a) Mössbauer spectra obtained at 50 K and corresponding fits (black lines). Eu^{3+} components centered around 1 mm/s are displayed as blue lines, whereas Eu^{2+} components close to −11 mm/s are depicted as red lines. (b) Mössbauer spectra obtained at 6.5 K and corresponding fits (black lines). Below the magnetic transition temperature, all components are subject to a hyperfine field. Moreover, two groups of Eu^{2+} sites with different hyperfine fields can be distinguished (solid and dashed red lines).

corresponding fit parameters are summarized in Table 5. The most prominent feature of all Mössbauer spectra at 50 K is the dominant absorption peak centered at approximately −11 mm/s indicating divalent Eu. Moreover, a significant Eu^{3+} contribution located around 1 mm/s is found in both the Cu- and the Au-containing compounds (see Figure 4a). Although contributing much less in the Ag-containing sample, Eu^{3+} has to be taken into account in order to achieve satisfactory fits at both temperatures. However, in this case, it was necessary to fix the line width of the Eu^{3+} component at 50 K. Considering the five different crystallographic Eu sites in these compounds, the pronounced line widths obtained are not surprising and are comparable to results obtained for other Zintl compounds with multiple Eu sites.[18]

Table 5. Isomer Shift, δ, Relative to EuF_3, Line Width Γ in mm/s, Hyperfine Field B_{hf} in T, and Relative Amount I_{rel} Obtained from ^{151}Eu Mössbauer Spectral Measurements at 50 and 6.5 K[a]

sample	T (K)	site	δ	Γ	B_{hf}	I_{rel}
CM = Cu	50	Eu^{2+}	−11.30(1)	3.4(2)		0.85(3)
		Eu^{3+}	1.20(3)	4(1)		0.15(3)
	6.5	Eu^{2+}	−11.10(1)	2.4(3)	2.3(4)	0.38
		Eu^{2+}	−11.20(2)	2.4	14.5(5)	0.47
		Eu^{3+}	1.20	4	3(2)	0.15
CM = Ag	50	Eu^{2+}	−11.10(1)	3.7(1)		0.94(2)
		Eu^{3+}	0.90(8)	4		0.06(2)
	6.5	Eu^{2+}	−12.10(3)	3.6(3)	12.4(7)	0.42
		Eu^{2+}	−11.11(2)	3.6	17.8(6)	0.52
		Eu^{3+}	0.90	4	4(2)	0.06
CM = Au	50	Eu^{2+}	−11.20(1)	3.2(2)		0.84(4)
		Eu^{3+}	1.20(5)	4(2)		0.16(4)
	6.5	Eu^{2+}	−11.20(3)	3.1(6)	4.4(8)	0.37
		Eu^{2+}	−11.00(3)	3.1	16.5(9)	0.47
		Eu^{3+}	1.20	4	6(3)	0.16

[a]A numeric value without error indicates that the corresponding parameter was fixed during fitting.

The shapes of the 6.5 K Mössbauer spectra (see Figure 4b) clearly suggest that from the Mössbauer perspective two distinct magnetically split Eu^{2+} sites are present in all compounds. Taking into account the low statistics due to the large absorption for the 21.4 keV X-rays, the following fitting strategy was employed for analysis of the 6.5 K spectra: relative Eu^{2+} intensities as determined from 50 K measurements were used, the isomer shift and line width of the Eu^{3+} component were fixed to their 50 K value, and the line widths of both Eu^{2+} components at 6.5 K were fit with a single parameter. In this way, spectra could be satisfactorily modeled by additionally assuming a ratio of 8:10 of both Eu^{2+} sites. This ratio roughly corresponds to the relative probability for a Eu ion to have no next-neighbor M and the probability to have at least one M next neighbor with M = Cu, Ag, and Au near neighbor, respectively (within a shell of 3.5 Å). Following this line of thought, the sublattice (A) of Eu ions with at least one near-neighbor M atom exhibits an increased Néel temperature or increased magnetic coupling compared to the sublattice (B) of Eu ions without next-neighbor M, resulting in an increased hyperfine field at sublattice A.

Although the relative Eu^{2+} and Eu^{3+} intensities based on 50 K measurements do not necessarily represent the actual, relative stoichiometry of both species because of a potentially different Lamb−Mössbauer factor, they agree with estimations based on magnetometry. Because the probability of the Mössbauer effect, for which the Lamb−Mössbauer factor is a measure, depends (among other factors) on the binding properties, different Eu sites and valencies can exhibit significantly different Lamb−Mössbauer factors. Accordingly, spectral intensities of different sites do not necessarily correspond to stoichiometry. The difference between the Eu^{3+} content in the Ag-containing compound and in the Au- and Cu-containing analogues is perfectly reproduced by Mössbauer spectroscopy. In all compounds, a small Eu^{3+} hyperfine field is observed. An alternative fit with a Eu^{3+} singlet results in unreasonably large line-width values, which is why the determination of a hyperfine field can be justified in these cases. Note that the observation of a hyperfine field for Eu^{3+} requires significant mixing of the diamagnetic $J = 0$ ground state with the $J = 1$ first excited state. Transferred hyperfine fields at Eu^{3+} were also observed in iron garnet[19] and Eu_3S_4[20] as well as in the Zintl phase $Eu_{14}MnP_{11}$,[18] which supports the assignment of a Eu^{3+} hyperfine field in the samples discussed herein. Reported Eu^{3+}-transferred fields at low temperatures range from about 5 T in Eu_3S_4[20] below 3.2 K and 33 T in $Eu_{14}MnP_{11}$ at 4.2 K.[18] Considering the distances between magnetic moments, which are 3.99 Å in the former and 3.58−3.82 Å in the latter compound, a correlation between the Eu^{2+}−Eu^{3+} distance and transferred field is likely. In this context, the rather small Eu^{3+} hyperfine fields fitted herein (see Table 5) are reasonable because Eu−Eu distances in these compounds (3.95−4.48 Å in the Cu-containing compound) are larger than those in Eu_3S_4. The observed broadening of the Eu^{3+} component cannot be accounted for consistently assuming

dx.doi.org/10.1021/ic502061w | Inorg. Chem. 2015, 54, 850−859

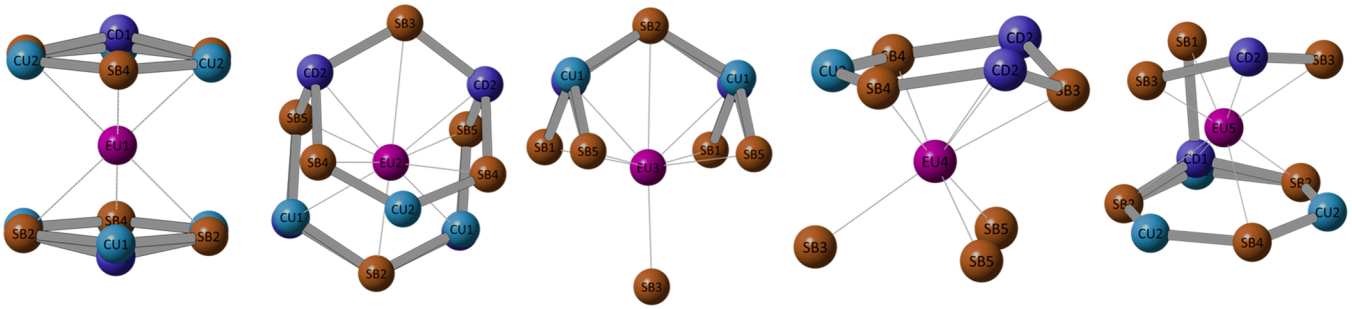

Figure 5. Five unique crystallographic Eu positions in $Eu_9Cd_{4-x}CM_{2+x-y}\square_ySb_9$ (a cutoff of 4 Å).

the presence of a Eu_3O_4 impurity phase[21] and, moreover, because the Eu^{2+} and Eu^{3+} sites are found to order simultaneously, Eu^{3+} should be considered an intrinsic feature of these compounds rather than an impurity phase. The same arguments can be made with respect to the $Eu_{14}MnPn_{11}$ compounds.[22]

A closer look at the structure in the vicinity of the Eu sites in order to provide for any possible crystallographic evidence of Eu^{3+} is shown in Figure 5 (4 Å cutoff). The environment of the Eu sites is different and does not show specific similarities or common features. The distances between the Eu ions and their nearest neighbors are listed in Table 6. On the basis of these distances, for all of the compounds of $Eu_9Cd_{4-x}CM_{2+x-y}\square_ySb_9$,

Table 6. Selected Bond Distances in the Neighbor of Five Crystallographic Eu Sites in $Eu_9Cd_{4-x}CM_{2+x-y}\square_ySb_9$

	Cu	Ag	Au
	Eu1		
Eu1−CM1 (×2)	3.4796	3.357	3.4763
Eu1−Sb2 (×4)	3.4078	3.4286	3.4292
Eu1−Sb4 (×2)	3.3973	3.4656	3.442
Eu1−CM2 (×4)	3.5557	3.5836	3.5436
	Eu2		
Eu2−CM2	3.1243	3.2171	3.1554
Eu2−Sb2	3.2952	3.2744	3.2841
Eu2−Sb4 (×2)	3.3247	3.3274	3.3295
Eu2−Sb5 (×2)	3.3156	3.3306	3.3301
Eu2−Cd2 (×2)	3.3605	3.3739	3.3676
	Eu3		
Eu3−Sb1 (×2)	3.2348	3.2444	3.2433
Eu3−Sb3	3.3235	3.3407	3.3221
Eu3−Cd1 (×2)	3.3338	3.3664	3.3579
Eu3−Sb5 (×2)	3.3713	3.3857	3.3838
Eu3−Eu4	3.9499	3.9453	3.952
	Eu4		
Eu4−CM2	3.1737	3.2102	3.2125
Eu4−Sb5 (×2)	3.3024	3.2993	3.3022
Eu4−Sb4 (×2)	3.3547	3.3584	3.3522
Eu4−Sb3	3.451	3.4579	3.46
Eu4−Sb3	3.5308	3.5364	3.5371
	Eu5		
Eu5−Sb3 (×2)	3.3355	3.3419	3.3524
Eu5−Cd1	3.3368	3.384	3.3675
Eu5−CM2 (×2)	3.4315	3.3938	3.425
Eu5−Sb4	3.3498	3.402	3.3679
Eu5−Sb2 (×2)	3.4889	3.5278	3.5059
Eu5−Sb1	3.5709	3.6194	3.6322
Eu5−Cd2	3.7983	3.7872	3.7929

the Eu2 and Eu3 sites show the shortest average Eu−Sb bonds. These short bonds can be evidence of higher positive charges at the Eu2 and Eu3 sites. These results are consistent with previous studies on $Yb_9Zn_4Bi_9$ that claimed that Yb2 and Yb3 are more positive compared to the other three Yb sites.[10] However, this historical verification in the 9−4−9 family[10,11] might not be valid because a comparison to the Ca analogue ($Ca_9Zn_{4.5}Sb_9$)[11] shows very similar trends in the average Ca−Sb bond lengths (see Figure 6). Therefore, because Ca cations

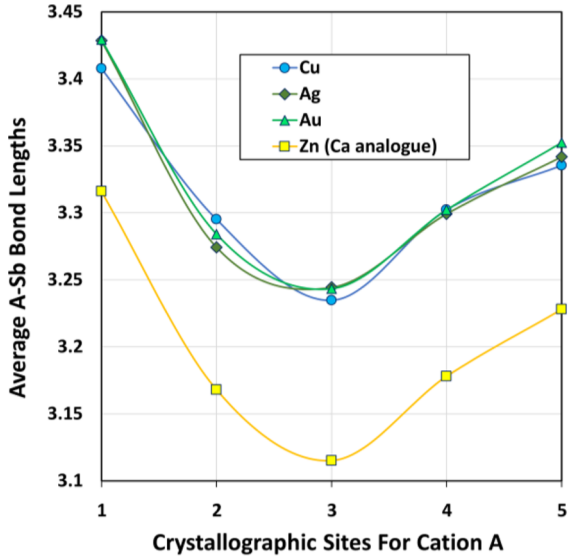

Figure 6. Average A−Sb bond lengths (A = Eu and Ca) at five crystallographic cation sites in $Eu_9Cd_{4-x}CM_{2+x-y}\square_ySb_9$ and $Ca_9Zn_{4.5}Sb_9$ compounds. Regardless of the type of the cation, the bond lengths follow the same trend.

can only have a 2+ oxidation state, the conclusion of higher positive charge >2 for these sites does not seem reasonable. It is more likely that these shorter distances are the result of other causes such as lower coordination numbers or covalence bonding interactions (a nonclassic interaction between the cation and anionic network in the Zintl phase context).

4. CONCLUSIONS

In this work, new compounds of $Eu_9Cd_{4-x}CM_{2+x-y}\square_ySb_9$ belonging to the 9−4−9 family of compounds were synthesized and structurally characterized by single-crystal X-ray diffraction. Their structures can be envisioned as a stuffed $Ca_9Mn_4Bi_9$ structure in which Cu, Ag, and Au coinage metals populate the interstitial position of the 4g site with 58.4, 56.0, and 51.0%, respectively. No specific trend is observed between the

dx.doi.org/10.1021/ic502061w | Inorg. Chem. 2015, 54, 850−859

occupation factors and size of the interstitial atom in contrast to previously reported members of this structure type that displays a strong correlation of the size and occupational fraction. In all of the structures, coinage metals show a trend to occupy the Cd1 site as well, however, with slight variation in the occupancy: 15%, 1.3%, and 10.6% for Cu, Ag, and Au coinage metals, respectively. The single-crystal X-ray diffraction associates a small fraction to Ag at Cd1 sites; however, this small fraction could be an artifact due to the low detection limit of X-ray diffraction techniques for distinguishing Cd^{2+} and Ag^{+} ions with the same number of electrons. EMPA resulted in compositions very similar to those obtained from single-crystal X-ray diffraction refinement for all samples but with a higher amount of Ag, as expected. In both interstitial and Cd1 sites, coinage metals hold a geometry close to trigonal-planar. The trend of the trigonal-planar environment by coinage metals can be evidence of the oxidation state of 1+ for coinage metals, as seen in EuCMSb compounds[16] in which CM^{1} ions locate at the center of a perfect trigonal plane made by three Sb ions. The structures can be viewed as being built up of polyanionic $[Cd_4Sb_9]^{19-}$, where the required electrons are provided by nine (Eu^{2+}) and one (CM^{+}), according to the Zintl concept, allowing all of the elements in the cationic and anionic subnetworks to reach the closed-shell electronic configuration according to the octet rule. This interpretation does not explain the bonding in $Eu_9Cd_{4-x}CM_{2+x-y}\square_ySb_9$ compounds because the magnetism and Mössbauer studies clearly show the presence of Eu^{3+} ions. The Cu- and Au-containing compounds show Eu^{3+} contents of ∼0.7 and 0.4/formula, respectively, through magnetism, whereas Ag did not show clear evidence of the presence of Eu^{3+} because it resulted in ∼8.9(3) Eu^{2+}/formula unit. Mössbauer studies showed clear evidence for the presence of Eu^{3+} in all samples including the Ag compound. The Cu- and Au-containing samples showed a very similar Eu^{3+} content of ∼1.3 Eu^{3+}/formula but higher than what magnetism revealed, which, however, can be attributed to presumably different Lamb−Mössbauer factors for Eu^{2+} and Eu^{3+}, respectively, leading to an overestimation of the Eu^{3+} content. The Ag-containing compound also shows a clear Eu^{3+} peak, which is suggestive of ∼0.4 Eu^{3+}/formula, which is within the standard deviation window of the number of Eu^{3+}/formula unit obtained by magnetism data, 0.1 (±3). In this study, the clear evidence of the presence of Eu^{3+} in $Eu_9Cd_{4-x}CM_{2+x-y}\square_ySb_9$ points to the limitations in the Zintl−Klemm concept because it cannot explain why these materials, given their chemical compositions and their crystal structures, adopt an electron configuration that clearly causes overpopulation of the bands above the Fermi level and formation of valence-imprecise compounds. Moreover, the Zintl−Klemm formalism does not explain the sources of the same anionic framework for both $Eu_9Cd_{4-x}CM_{2+x-y}\square_ySb_9$ and other members in the 9−4−9 family like in $Ca_9Zn_{4.5}Sb_9$ while they adopt different numbers of electrons because in many cases only an oxidation state of 2+ for the cation is possible.

The possible flexibility in air-stable structures of $Eu_9Cd_{4-x}CM_{2+x-y}\square_ySb_9$ in tolerating a small variation in their compositions, and consequently in their electronic properties, makes them ideal candidates for thermoelectric applications. Moreover, the highly disordered structures resulting from partial occupation at the interstitial site and splitting of the Cd1 site with fractional occupation at the second position by coinage metals with considerable mass fluctuation (compare the Cu and Au masses with that of Cd) are all promising features that should provide the very low thermal conductivities required in thermoelectric materials. The call for studying their potential thermoelectric applications becomes more inviting because the new thermoelectric studies on the $Yb_9Mn_{4+x}Sb_9$ sample[23] have shown very low thermal conductivity (k_L < 0.4 W/mK) with a high thermoelectric figure of merit of zT = 0.7 at 950 K, comparable to the state of the art $Yb_{14}MnSb_{11}$.[24]

■ ASSOCIATED CONTENT

Supporting Information

Elemental X-ray maps of the single crystals used for magnetic studies along with the X-ray crystallographic files (in CIF format) for the $Eu_9Cd_{4-x}CM_{2+x-y}\square_ySb_9$ (CM = Cu, Ag, and Au) structures. This material is available free of charge via the Internet at http://pubs.acs.org.

■ AUTHOR INFORMATION

Corresponding Author

*E-mail: smkauzlarich@ucdavis.edu.

Notes

The authors declare no competing financial interest.

■ ACKNOWLEDGMENTS

We thank Dr. Sarah Roeske and Nick Botto for assistance with microprobe analysis, Peter Klavins for assistance with the magnetic measurements, and Dr. Svilen Bobev for many helpful discussions. This research was funded by a Summer GSR fellowship for N.K., GAANN fellowship 24NKKSM, and NSF Grant DMR-1100313. We also acknowledge support from DFG through the SPP1386 program.

■ REFERENCES

(1) Miller, G. J.; Schmidt, M. W.; Wang, F.; You, T.-S. Quantitative Advances in the Zintl−Klemm Formalism. *Zintl Phases: Principles and Recent Developments*; Springer-Verlag: Berlin, 2011.
(2) Kauzlarich, S. M. *Chemistry, Structure, and Bonding of Zintl Phases and Ions*; VCH Publishers, Inc.: New York, 1996.
(3) Kazem, N.; Xie, W.; Ohno, S.; Zevalkink, A.; Miller, G. J.; Snyder, G. J.; Kauzlarich, S. M. *Chem. Mater.* **2014**, *26*, 1393−1403.
(4) Cox, C. A.; Toberer, E. S.; Levchenko, A. A.; Brown, S. R.; Snyder, G. J.; Navrotsky, A.; Kauzlarich, S. M. *Chem. Mater.* **2009**, *21*, 1354−1360.
(5) Toberer, E. S.; Brown, S. R.; Ikeda, T.; Kauzlarich, S. M.; Snyder, G. J. *J. Appl. Phys.* **2008**, *93*, 062110-1−062110-3.
(6) Cao, Q.; Zhang, H.; Tang, M.; Chen, H.; Yang, X.; Grin, Y.; Zhao, J. *J. Appl. Phys.* **2010**, *107*, 053714-1−053714-5.
(7) Kauzlarich, S. M.; Brown, S.; Snyder, G. J. *Dalton Trans.* **2007**, 2099−2107.
(8) Toberer, E. S.; May, A. F.; Snyder, G. J. *Chem. Mater.* **2010**, *22*, 624−634.
(9) (a) Brechtel, E.; Cordier, G.; Schäfer, H. *Z. Naturforsch.* **1979**, *34B*, 1229−1233. (b) Brechtel, E.; Cordier, G.; Schäfer, H. *Z. Naturforsch.* **1981**, *36B*, 1099−1104.
(10) Kim, S. J.; Salvador, J.; Bilc, D.; Mahanti, S. D.; Kanatzidis, M. G. *J. Am. Chem. Soc.* **2001**, *123*, 12704−12705.
(11) Bobev, S.; Thompson, J. D.; Sarrao, J. L.; Olmstead, M. M.; Hope, H.; Kauzlarich, S. M. *Inorg. Chem.* **2004**, *43*, 5044−5052.
(12) Xia, S.-q.; Bobev, S. *J. Am. Chem. Soc.* **2007**, *129*, 10011−10018.
(13) Xia, S.-Q.; Bobev, S. *Chem. Mater.* **2009**, *22*, 840−850.
(14) Canfielda, P. C.; Fiska, Z. *Philos. Mag. B* **1992**, *65*, 1117−1123.
(15) Saparov, B.; Bobev, S.; Ozbay, A.; Nowak, E. R. *J. Solid State Chem.* **2008**, *181*, 2690−2696.
(16) Schuster, U. H.; Tomuschat, C. *Z. Naturforsch.* **1978**, *33B*, 983−986.

(17) Mantina, M.; Valero, R.; Cramer, C. J.; Truhlar, D. G. *CRC Handbook of Chemistry and Physics*; CRC Press: London, 2013.
(18) Hermann, R. P.; Grandjean, F.; Kafle, D.; Brown, D. E.; Johnson, C. E.; Kauzlarich, S. M.; Long, G. J. *Inorg. Chem.* **2007**, *46*, 10736−10740.
(19) Stachel, M. M.; Hufner, S.; Crecelius, G.; Quitmann, D. *Phys. Lett.* **1968**, *28A*, 188−200.
(20) Massenet, O.; Coey, J. M.; Holtzberg, F. *J. Phys. (Paris)* **1976**, *37*, 297−300.
(21) Wickman, H. H.; Catalano, E. *J. Appl. Phys.* **1968**, *39*, 1248−1249.
(22) Hermann, R. P.; Grandjean, F.; Kauzlarich, S. M.; Jiang, J.; Brown, S.; Long, G. J. *Inorg. Chem.* **2004**, *43*, 7005−7013.
(23) Bux, S. K.; Zevalkink, A.; Janka, O.; Uhl, D.; Kauzlarich, S.; Snyder, J. G.; Fleurial, J.-P. *J. Mater. Chem. A* **2014**, *2*, 215−220.
(24) Brown, S. R.; Kauzlarich, S. M.; Gascoin, F.; Snyder, G. J. *Chem. Mater.* **2006**, *18*, 1873−1877.